# ADAPTIVE TOTAL VARIATIONAL REGULARIZATION OF GAUSSIAN DENOISERS FOR MULTIPLICATIVE NOISE REMOVAL

Kehan Shi

Department of Mathematics, China Jiliang University
Hangzhou 310018, China
Computational Imaging Group and Helmholtz Imaging
Deutsches Elektronen-Synchrotron DESY, 22607 Hamburg, Germany

Abstract. In this paper, a convex variational model based on the adaptive total variation (TV) regularization is proposed for image restoration under multiplicative noise. The adaptive weight allows for greater smoothing in the bright region for the suppression of speckles. The model includes a nonconvex data fidelity term and also a quadratic penalty term that enforces the restored image to be close to a reference image deduced from a Gaussian denoiser. It can be viewed as the adaptive TV regularization of the Regularization by Denoising (RED) approach for multiplicative noise removal. We prove that the model admits a unique minimizer in a suitable function space and provide a fast numerical algorithm based on the alternating direction method with multipliers (ADMM) for it. Different Gaussian denoisers, including the patch-based algorithm BM3D and the learning-based algorithm DnCNN, are considered for the model in numerical experiments. It is shown that our model efficiently removes multiplicative noise without introducing artifacts.

1. **Introduction.** Image restoration is a basic and widely studied topic in image processing. This paper considers the problem of image restoration under multiplicative noise, which occurs in images obtained from coherent imaging systems, e.g., synthetic aperture radar (SAR) [18], ultrasound imaging [29], and laser imaging [21]. The image degradation model is given by

$$f = u_0 n,$$

where $u_0$ denotes the original noise-free image and $f$ denotes the observed image contaminated by the noise $n$. In this paper, we assume that $f$ is a $L$-look image obtained from SAR by the multi-look averaging technique. Then $n$ follows a Gamma distribution with mean 1, variance $1/L$, and the probability density function

$$P(x) = \frac{L^L}{\Gamma(L)} x^{L-1} \exp(-Lx), \quad x \geq 0,\ L \geq 1,$$

where $\Gamma(\cdot)$ is the usual Gamma function. Figure 1 shows the test image Cameraman with Gamma multiplicative noise. We observe the signal-dependent nature of the noise. More precisely, the higher the gray level of $u_0$ is, the more remarkable the influence of the noise is.

2020 *Mathematics Subject Classification.* 68U10, 94A08.

*Key words and phrases.* Image restoration, multiplicative noise, adaptive TV regularization, Gaussian denoiser.

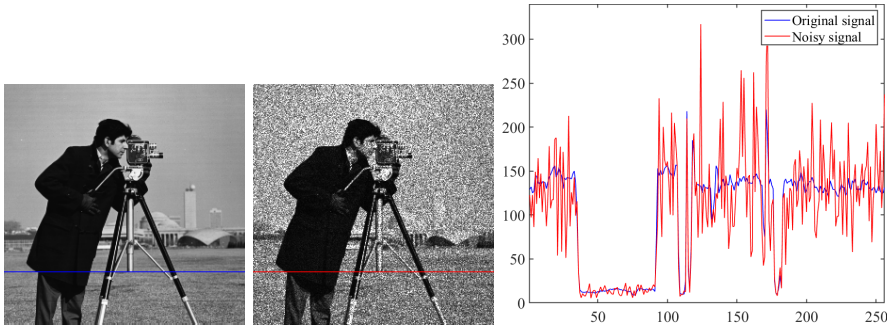


FIGURE 1. The test image Cameraman and the noisy image corrupted by multiplicative noise with $L = 10$. The blue line and red line present the gray value of the original image and the noisy image on the 200th row respectively.

Many methods have been proposed for the problem of image restoration under multiplicative noise. Generally, they can be categorized as the variational method, the patch-based method, the learning-based method, etc. In the recent paper [13], the authors presented a detailed overview on this topic. Given this, we recall a few variational image denoising models that are closely related to our work in the following and refer the readers to [13] for other approaches.

A variational model for image restoration usually consists of a regularization term and a data fidelity term. In [1], the authors proposed to combine the famous total variation (TV) regularization [20] with a data fidelity term that is deduced by using the maximum a posteriori (MAP) estimator for the multiplicative Gamma noise. This leads to the AA model

$$\min_u \int_\Omega |\nabla u| dx + \eta \int_\Omega \left( \log u + \frac{f}{u} \right) dx, \tag{1}$$

where $\eta$ is a positive constant.

The data fidelity term of functional (1) is noncovex. The authors of [12] suggested to add a quadratic penalty term that includes the statistical information of multiplicative noise and proposed the model

$$\min_u \int_\Omega |\nabla u| dx + \eta \int_\Omega \left( \log u + \frac{f}{u} \right) dx + \mu \int_\Omega \left( \sqrt{\frac{u}{f}} - 1 \right)^2 dx. \tag{2}$$

It becomes convex for a large penalty parameter $\mu > 0$. On the other hand, AA model can also be improved in terms of the regularization term. The authors of [33] proposed to utilize the adaptive Euler's elastica regularization and a convex data fidelity term [25] for multiplicative noise removal, which reads

$$\min_u \int_\Omega \left( \alpha + b \left( \operatorname{div} \left( \frac{\nabla u}{|\nabla u|} \right) \right)^2 \right) |\nabla u| dx + \eta \int_\Omega (u - f \log u) \, dx. \tag{3}$$

Here $b$ is a positive constant and $\alpha$ is an adaptive function (also known as the gray level indicator [11, 17, 14, 23]) given by

$$\alpha(x) = \frac{|f_\sigma(x)|^p}{|\max_{x \in \Omega} f_\sigma(x)|^p}, \quad p > 0, \tag{4}$$

where $f_\sigma = G_\sigma * f$ and $G_\sigma = \frac{1}{2\pi\sigma^2} e^{-\frac{|x|^2}{2\sigma^2}}$ is the Gaussian kernel. If $\alpha$ is a positive constant, then the first term in (3) is just the usual Euler's elastica regularization [24]. If $b \equiv 0$, we have the adaptive TV regularization [26]. It has been shown that model (3) is able to restore small geometrical structures in images.

The variational method has attracted a lot of attention in image processing. There are two main reasons for this. Firstly, variational models generally have good theoretical properties and fast numerical solvers. For example, the TV regularization has been studied in the space of functions of bounded variation, which requires no differentiability or even continuity of the function [2]. Optimization algorithms, including the split-Bregman algorithm [15], the primal-dual algorithm [5], the alternating direction method with multipliers (ADMM) [3], et al., have been developed for solving non-smooth (and nonconvex) variational models efficiently. Secondly, variational models have strong flexibility and interpretability to handle various image processing problems. Different data fidelity terms have been considered for different tasks, for example, image deblurring [32], image inpainting [6], and Cauchy noise removal [22]. Let us go back to model (1) and model (3). A direct calculation implies that the gradient flows of them contain reaction terms $\frac{f-u}{u^2}$ and $\frac{f-u}{u}$ respectively. The denominators $u^2$ and $u$ fit the signal-dependent nature of multiplicative noise.

Recently, the shortcoming of the variational method has become apparent. With the emergence of many new methods, the image processing performance of the variational method is less attractive. Although the variational method has advantages in handling cartoon images and piecewise homogeneous images, it is surpassed by the patch-based method [9] and the learning-based method [31] for dealing natural images.

In this paper, we propose a simple but effective approach to improve the performance of the traditional variational model for image restoration under multiplicative noise. This is achieved by introducing an additional quadratic penalty term, resulting in a convex variational model. The penalty term ensures that the minimizer of the variational model is close to a reference image deduced by applying a sophisticated Gaussian denoiser to the noisy image. Since the model is convex, it has fine mathematical properties and can be solved efficiently by algorithms like ADMM. Generally, a Gaussian denoiser with fixed parameters cannot effectively handle the bright region (i.e., the region that is heavily contaminated) and the dark region (i.e., the region that is lightly contaminated) of the noisy image simultaneously. We propose to update the reference image through an iterative process to achieve the desired image restoration results.

The new quadratic penalty term has a close connection with the Regularization by Denoising (RED) method [19], which uses an image denoiser to construct the regularization term and solves inverse problems in image processing, e.g., image deblurring and image super-resolution, effectively. From this perspective, we could regard the proposed model as the adaptive TV regularization of RED for multiplicative noise removal. Different from the traditional variational method, the proposed energy functional is well-posed even without the regularization term. The adaptive TV term suppresses speckles in images by allowing greater smoothing in the bright region and avoids artifacts introduced by the Gaussian denoiser.

This paper is organized as follows. In section 2, we state the proposed variational model for multiplicative noise removal and discuss its properties. In section 3, we

discuss the numerical implementation of the model. Experimental simulations are presented in section 4. We conclude the paper in section 5.

## 2. Adaptive TV regularization of Gaussian denoisers for multiplicative denoising.

In this section, we propose a new convex variational model for the removal of multiplicative noise and study the existence and uniqueness of solutions to the model. We also discuss the relationship of the proposed model to several existing models.

### 2.1. The proposed model.

Let $\mathcal{D}$ be an image denoiser for Gaussian noise. Since the variational method is considered in the continuous setting, we assume that $\Omega \subset \mathbb{R}^2$ is the image domain, $\mathcal{D}$ is an operator on the Lebesgue space $L^\infty(\Omega)$, and $f \in L^\infty(\Omega)$. By applying the denoiser $\mathcal{D}$ to the given noise image $f$, we obtain a reference image

$$g := \mathcal{D}(f).$$

Then the proposed variational model for image restoration under multiplicative noise is as follows

$$\min_u E(u) := \int_\Omega \alpha(x)|\nabla u| dx + \frac{\mu}{2}\int_\Omega |u-g|^2 dx + \eta \int_\Omega \left(\log u + \frac{f}{u}\right) dx, \qquad (5)$$

where $\mu$, $\eta$ are two positive constants and $\alpha(x)$ is an adaptive function given by (4).

The first term in $E(u)$ is an adaptive TV regularization. As we have mentioned, the signal-dependent nature of multiplicative noise reveals the fact that the higher the gray level of the image, the greater the influence of the noise. By introducing $\alpha(x)$, we adaptively control the strength of regularization. The second $L^2$ penalty term enforces the restored image to be close to the reference image $g$. It also makes the energy functional strictly convex if $\mu$ satisfies a certain condition. The third fidelity term comes from the MAP estimator for the multiplicative noise.

The minimizer of energy functional $E$ depends on the reference image $g$ and thus on the denoiser $\mathcal{D}$. Consequently, we could take full advantage of recent impressive achievements in Gaussian noise removal to handle the problem of multiplicative noise removal without modifying the denoiser $\mathcal{D}$. Similar idea that deploying off-the-shelf image denoisers to solve other inverse problems in image processing has been proposed in [28, 19]. Since $\mathcal{D}$ is designed for Gaussian denoising, it is expected that the solution of (5) does not give a convincing result for our problem. An iterative procedure is required. We leave it to section 3.

### 2.2. Roles of $\alpha(x)$ and $\mu$.

The proposed model (5) covers three image restoration models as its special cases. Let $\alpha(x)$ be a constant function and $\mu = 0$. Model (5) is nothing but the AA model (1). If $\alpha(x)$ is given by (4) and $\mu = 0$, model (5) becomes the adaptive AA model. A similar model is considered in [33] for the removal of multiplicative noise. The third case that $\alpha(x) \equiv 0$ and $\mu \neq 0$ is nontrivial. To illustrate it, let us review the image restoration method of Regularization by Denoising (RED) [19].

In RED, the regularization term in a variational model is replaced by

$$R(u) := \frac{1}{2}\int_\Omega u(u - \mathcal{D}(u)) dx,$$

where $\mathcal{D}$, like above, is a Gaussian denoiser. Combing $R(u)$ with the data fidelity term of the AA model leads to

$$\min_u \frac{1}{2}\int_\Omega u(u-\mathcal{D}(u))dx + \eta\int_\Omega \left(\log u + \frac{f}{u}\right)dx. \tag{6}$$

Although the establishment of model (6) for multiplicative noise removal follows directly from the basic idea of [19], the model is new in the literature as far as we know.

Generally, it is difficult to analyze properties for $R(u)$ since the unknown structure of the denoiser $\mathcal{D}$. But under certain assumptions on $\mathcal{D}$, the authors showed that $R(u)$ is convex [19]. More importantly, the Euler-Lagrange equation of (6) is given by

$$0 = u - \mathcal{D}(u) + \eta\frac{f-u}{u^2}.$$

By using the fixed point strategy, the above equation can be solved iteratively through

$$0 = u^{(k+1)} - \mathcal{D}(u^{(k)}) + \eta\frac{f-u^{(k+1)}}{(u^{(k+1)})^2}, \quad k = 0, 1, 2\cdots \tag{7}$$

for the given initial guess $u^{(0)} = f$. We observe that equation (7) with $k = 0$ turns out to be the Euler-Lagrange equation of (5) with $\alpha(x) \equiv 0$ and $\mu = 1$.

The above result reveals that the derivative of the quadratic penalty term in (5) is equivalent to one step of the fixed point scheme for RED regularization term $R(u)$. Consequently, the proposed model (5) can be viewed as the combination of the adaptive TV model and RED. The successful experience of RED gives us the reason to believe that the proposed model (5) can effectively handle multiplicative noise if we take an iterative procedure similar to (7) for it.

2.3. **Properties.** Throughout this section, we assume that $\Omega \subset \mathbb{R}^n$, $n \geq 2$, is a bounded domain with Lipschitz boundary. The given data $f(x)$, $g(x) \in L^\infty(\Omega)$ with $\inf_\Omega f(x) > 0$ and $\inf_\Omega g(x) > 0$. Then the adaptive function $\alpha(x) \in C^\infty(\overline{\Omega}, \mathbb{R}^+)$. In the following, we show that (5) is strictly convex. Consequently, it admits a unique solution in a proper function space.

**Lemma 2.1.** *If $\frac{\eta}{\mu} \leq 27\inf_\Omega |f|^2$, the energy functional $E(u)$ defined in (5) is strictly convex.*

*Proof.* We only need to prove that

$$\frac{\mu}{2}\int_\Omega |u-g|^2 dx + \eta\int_\Omega \left(\log u + \frac{f}{u}\right)dx$$

is strictly convex since the adaptive TV regularization $\int_\Omega \alpha(x)|\nabla u|dx$ is convex.

Let $x \in \Omega$ be fixed. We define a function $h(t)$ as

$$h(t) = \frac{\mu}{2}(t-g(x))^2 + \eta\left(\log t + \frac{f(x)}{t}\right), \quad t \in \mathbb{R}^+.$$

By direct computation,

$$h''(t) = \mu + \eta\frac{2f(x)-t}{t^3}.$$

We observe that $t^3h''(t)$ admits its unique minimum at $t = (\frac{\eta}{3\mu})^{1/2}$. Consequently, if

$$\left(\frac{\eta}{3\mu}\right)^{3/2} h''\left(\left(\frac{\eta}{3\mu}\right)^{1/2}\right) = \mu\left(\frac{\eta}{3\mu}\right)^{3/2} + \eta\left(2f(x) - \left(\frac{\eta}{3\mu}\right)^{1/2}\right) \geq 0,$$

i.e., $\frac{\eta}{\mu} \leq 27|f(x)|^2$, $h''(t) \geq 0$ and $h$ is strictly convex. □

The functional (5) is minimized in the space of functions of bounded variation (BV). A brief review of the solution space is in order. More details can be founded in [7, 4].

Let $u \in L^1(\Omega)$. The $\alpha$-total variation ($\alpha$-TV) of $u$ is as follows

$$\int_\Omega \alpha|\nabla u| = \sup\left\{\int_\Omega u \mathrm{div}\varphi dx : \varphi \in C_0^1(\Omega;\mathbb{R}^N),\ |\varphi_i(x)| \leq \alpha(x) \text{ for } x \in \Omega\right\},$$

where $\varphi = (\varphi_1, \varphi_2, \cdots, \varphi_n)$ is a vector-valued function. We define $BV_\alpha(\Omega)$ as the subspace of $u \in L^1(\Omega)$ such that the $\alpha$-TV of $u$ is finite. The space $BV_\alpha(\Omega)$ equipped with the norm $\|u\|_\alpha = \|u\|_{L^1(\Omega)} + \int_\Omega \alpha|\nabla u|$ is a Banach space. Moreover, the $\alpha$-TV is lower semicontinuous.

**Lemma 2.2.** *Let $u_n \in BV_\alpha(\Omega)$ and $u_n \to u$ in $L^1(\Omega)$ as $n \to +\infty$. Then*

$$\int_\Omega \alpha|\nabla u| \leq \liminf_{n\to\infty} \int_\Omega \alpha|\nabla u_n|.$$

At last, we mention that the classical space $BV(\Omega)$ is defined by taking $\alpha \equiv 1$ in the definition of $BV_\alpha(\Omega)$. Given the above preliminaries, we now prove that model (5) admits a unique minimizer in $S(\Omega) := \{u | u \in BV(\Omega), u > 0\}$.

**Theorem 2.3.** *Problem (5) has at least one solution $u \in S(\Omega)$ satisfying*

$$\min\left(\inf_\Omega f, \inf_\Omega g\right) \leq u \leq \max\left(\sup_\Omega f, \sup_\Omega g\right). \tag{8}$$

*Moreover, if $\frac{\eta}{\mu} \leq 27 \inf_\Omega |f|^2$, the solution is unique.*

*Proof.* Let $c_1(x) := \min(f(x), g(x))$, $c_2(x) := \max(f(x), g(x))$, $d_1 := \inf_\Omega c_1$, and $d_2 := \sup_\Omega c_2$. Since $E(u)$ is lower bounded, there exists a minimizing sequence $\{u_i\}_{i=1}^\infty \subset S(\Omega)$ for problem (5).

Let $x \in \Omega$ be fixed and

$$h(t) = \frac{\mu}{2}(t - g(x))^2 + \eta\left(\log t + \frac{f(x)}{t}\right), \quad t \in \mathbb{R}^+.$$

Then $h(t)$ is decreasing if $t \in (0, c_1(x))$ and increasing if $t \in (c_2(x), +\infty)$. Consequently,

$$h(\min(t, c_2(x))) \leq h(t),$$

which leads to

$$F(\inf(u, d_2)) \leq F(u), \tag{9}$$

where

$$F(u) := \frac{\mu}{2}\int_\Omega |u - g|^2 dx + \eta \int_\Omega \log u + \frac{f}{u} dx.$$

Recalling the definition of $\alpha$-TV and the fact that $u > 0$, we have

$$\int_\Omega \alpha|\nabla \inf(u, d_2)| \leq \int_\Omega \alpha|\nabla u|. \tag{10}$$

We deduce from (9)–(10) that

$$E(\inf(u, d_2)) \leq E(u).$$

In the same way we obtain

$$E(\sup(u, d_1)) \leq E(u).$$

Consequently, we can always assume that $d_1 \le u_i \le d_2$, $1 \le i < \infty$.

Since $\{u_i\}_{i=1}^{\infty}$ is a minimizing sequence, we know that both $F(u_i)$ and $\int_\Omega \alpha|\nabla u|$ are bounded. By $\int_\Omega |\nabla u| \le \frac{1}{\min \alpha}\int_\Omega \alpha|\nabla u|$, we further have $\{u_i\}_{i=1}^{\infty} \subset BV(\Omega)$. Recalling the compactness of $BV(\Omega)$, there exist a subsequence of $\{u_i\}_{i=1}^{\infty}$ (still denoted by itself) and a function $u \in BV(\Omega)$, such that

$$u_i \to u, \quad \text{in } L^1(\Omega),$$

and (8) holds. By the lower semicontinuity of the $\alpha$-TV and Fatou's lemma, we obtain that $u$ is a solution of problem (5).

The uniqueness of the solution follows directly from the strict convexity of $E(u)$. □

## 3. Numerical implementation.

In this section, we present a numerical algorithm based on the alternating direction method with multipliers (ADMM) [3] for minimizing the functional $E(u)$ defined in (5). We also discuss details of the proposed model for multiplicative noise removal.

### 3.1. ADMM algorithm.

To simplify the notation, we use the same notation for both the continuous contest and the discrete contest. Let $f \in \mathbb{R}^{MN}$ be the given noisy image. The discrete $\alpha$-total variation of $u$ is defined as

$$|\nabla u|_\alpha = \sum_{i,j=1}^{MN} \alpha_{i,j}\sqrt{(\partial_x^+ u)_{i,j}^2 + (\partial_y^+ u)_{i,j}^2},$$

where $\nabla u := (\partial_x^+ u, \partial_y^+ u)^T$ is the forward finite difference approximation of the gradient operator with periodic boundary condition,

$$(\partial_x^+ u)_{i,j} = \begin{cases} u_{i+1,j} - u_{i,j}, & \text{if } 1 \le i < M, \\ u_{1,j} - u_{M,j}, & \text{if } i = M, \end{cases} \quad (\partial_y^+ u)_{i,j} = \begin{cases} u_{i,j+1} - u_{i,j}, & \text{if } 1 \le j < N, \\ u_{i,1} - u_{i,N}, & \text{if } j = N. \end{cases}$$

Similarly, we define the backward finite difference operators

$$(\partial_x^- u)_{i,j} = \begin{cases} u_{i,j} - u_{i-1,j}, & \text{if } 1 < i \le M, \\ u_{1,j} - u_{M,j}, & \text{if } i = 1, \end{cases} \quad (\partial_y^- u)_{i,j} = \begin{cases} u_{i,j} - u_{i,j-1}, & \text{if } 1 < j \le N, \\ u_{i,1} - u_{i,N}, & \text{if } j = 1, \end{cases}$$

and the discrete divergence operator

$$(\mathrm{div} p)_{i,j} = (\partial_x^- p_1)_{i,j} + (\partial_y^- p_2)_{i,j},$$

for any $p = (p_1, p_2)$.

The discrete version of the proposed model (5) is given as

$$\min_{u \in \mathbb{R}^{MN}} |\nabla u|_\alpha + \frac{\mu}{2}\|u - g\|_2^2 + \eta(\log u + \frac{f}{u}, 1), \tag{11}$$

where $\|\cdot\|_2$ and $(\cdot,\cdot)$ are the norm and the inner product of $l^2$. We solve it numerically by the augmented Lagrangian method. For this, we introduce auxiliary variables $p$ and $v$ and rewrite (11) as the equivalent form

$$\begin{aligned} &\min_u |p|_\alpha + \frac{\mu}{2}\|u - g\|_2^2 + \eta(\log v + \frac{f}{v}, 1), \\ &\text{s.t. } p = \nabla u, \ v = u, \end{aligned}$$

which is a constrained optimization problem. The corresponding augmented Lagrangian functional is defined as

$$\begin{aligned} L(u,p,v;\lambda_1,\lambda_2) = |p|_\alpha + \frac{\mu}{2}\|u-g\|_2^2 + \eta(\log v + \frac{f}{v},1) + (\lambda_1, p-\nabla u) \\ + \frac{r_1}{2}\|p-\nabla u\|_2^2 + (\lambda_2, v-u) + \frac{r_2}{2}\|v-u\|_2^2, \end{aligned} \tag{12}$$

where $\lambda_1$ and $\lambda_2$ are the Lagrange multipliers, $r_1$ and $r_2$ are positive constants. Then the alternating iterative algorithm for minimizing (12) is described in the following Algorithm 1.

**Algorithm 1** Solving (11) by ADMM.

**Require:** Images $f$ and $g$, weight $\alpha$, constants $\mu$, $\eta$, $r_1$, $r_2$, and $\varepsilon$.
Initialization: $k=0$, $v^0$ and $\lambda_2^0$ are null vectors, $p^0$ and $\lambda_1^0$ are null matrices.
**while** $\frac{|E(u^k)-E(u^{k-1})|}{|E(u^k)|} < \varepsilon$ is not satisfied **do**
Update subproblems:

$$u^{k+1} = \arg\min_u L(u, p^k, v^k; \lambda_1^k, \lambda_2^k); \tag{13}$$

$$p^{k+1} = \arg\min_p L(u^{k+1}, p, v^k; \lambda_1^k, \lambda_2^k); \tag{14}$$

$$v^{k+1} = \arg\min_v L(u^{k+1}, p^{k+1}, v; \lambda_1^k, \lambda_2^k). \tag{15}$$

Update Lagrange multipliers:

$$\lambda_1^{k+1} = \lambda_1^k + r_1(p^{k+1} - \nabla u^{k+1});$$
$$\lambda_2^{k+1} = \lambda_2^k + r_2(v^{k+1} - u^{k+1}).$$

Update $k = k+1$.
Calculate the energy $E(u^k)$ by (11).
**end while**
**return** $u^k$.

3.2. **Solutions of subproblems.** Three subproblems (13)–(15) are needed to be solved for Algorithm 1. We discuss the solutions for them in the following.

By substituting $L$ defined in (12) into (13) and ignoring trivial terms, we arrive at the $u$-subproblem

$$u^{k+1} = \arg\min_u \frac{\mu}{2}\|u-g\|_2^2 + (\lambda_1^k, -\nabla u) + \frac{r_1}{2}\|p^k - \nabla u\|_2^2 + (\lambda_2, -u) + \frac{r_2}{2}\|v^k - u\|_2^2.$$

Then $u^{k+1}$ is the solution of the linear system

$$-r_1 \mathrm{div}\nabla u + \mu u + r_2 u = -\mathrm{div}\lambda_1^k - r_1 \mathrm{div} p^k + \lambda_2 + \mu g + r_2 v^k.$$

Since periodic boundary condition is imposed, it can be solved efficiently by the fast Fourier transform. More precisely,

$$u^{k+1} = \mathcal{F}^{-1}\left(\frac{\mathcal{F}(-\mathrm{div}\lambda_1^k - r_1\mathrm{div}p^k + \lambda_2 + \mu g + r_2 v^k)}{-r_1\mathcal{F}(\Delta) + \mu + r_2}\right), \tag{16}$$

where $\mathcal{F}$ and $\mathcal{F}^{-1}$ denote the fast Fourier transform (FFT) and its inverse transform, respectively. More details on the calculation of $\mathcal{F}(\Delta)$ can be founded in [27].

For the $p$-subproblem (14), it can be recast as

$$p^{k+1} = \arg\min_p |p|_\alpha + (\lambda_1^k, p) + \frac{r_1}{2}\|p - \nabla u^{k+1}\|_2^2.$$

We rewrite it as

$$p^{k+1} = \arg\min_p |p|_\alpha + \frac{r_1}{2}\left\|p - \left(\nabla u^{k+1} - \frac{\lambda_1^k}{r_1}\right)\right\|_2^2,$$

and use the soft shrinkage operator [15] to find the closed-form solution

$$p^{k+1} = \text{shrinkage}\left(\nabla u^{k+1} - \frac{\lambda_1^k}{r_1}, \frac{\alpha}{r_1}\right), \tag{17}$$

where

$$\text{shrinkage}(x, y) = \text{sign}(x) \cdot \max(|x| - y, 0).$$

At last, let us consider the $v$-subproblem (15), which has the following form

$$v^{k+1} = \arg\min_v \eta(\log v + \frac{f}{v}, 1) + (\lambda_2^k, v) + \frac{r_2}{2}\|v - u^{k+1}\|_2^2.$$

The optimality condition for it is given by

$$\eta\frac{v - f}{v^2} + \lambda_2^k + r_2(v - u^{k+1}) = 0, \tag{18}$$

which has the second derivative and can be solved by the Newton method.

In the proposed model (5), the given image $g$ represents an approximation of $u$ deduced from a Gaussian denoiser. Since the variable $v$ in the ADMM scheme is also used for the approximation of $u$, we are able to approximate equation (18) by

$$\eta\frac{v - f}{g^2} + \lambda_2^k + r_2(v - u^{k+1}) = 0,$$

which is a linear equation and has the solution

$$v^{k+1} = \frac{r_2 u^{k+1} - \lambda_2^k + \eta f/g^2}{\eta/g^2 + r_2}.$$

3.3. **Multiplicative noise removal algorithm.** The proposed model (5) includes a reference image $g$ that is deduced from a Gaussian denoiser. Consequently, the restoration result of model (5) relies on the Gaussian denoiser we utilize. A Gaussian denoiser usually has at least one free parameter for controlling the strength of denoising. Since the parameter depends on the standard deviation of the Gaussian noise $\sigma$, we regard $\sigma$ as the only parameter of $\mathcal{D}$ and use the notation $\mathcal{D}_\sigma$. It should be noticed that the restoration result of (5) depends heavily on the choice of $\sigma$.

The denoiser $\mathcal{D}_\sigma$ is not designed for multiplicative noise removal. We could see that $g = \mathcal{D}_\sigma(f)$ can not give a satisfied image restoration result, especially when the multiplicative noise level is high. As a consequence, the solution of model (5) is not what we expect. To solve this problem, we follow the idea of RED which utilizes an iterative procedure to update $g$. The proposed algorithm for image restoration under multiplicative noise is summarized in the following Algorithm 2.

In the 5th step, the parameter $\sigma_1$ for $\mathcal{D}$ is not a constant, but a function of $i$. As the parameter $i$ increases, we can expect that the high-frequency noise in the image is removed. We naturally want the parameter $\sigma_1$ to be a decreasing function of $i$ to reduce the denoising strength of $\mathcal{D}$. Algorithm 2 contains a few free parameters that affect the image restoration performance. We introduce a post-processing step in the 14th step, which makes it easier to select these parameters.

**Algorithm 2** Multiplicative noise removal by model (5).

**Require:** Noisy image $f$, denoiser $\mathcal{D}$, parameters $\mu$, $\eta$, $r_1$, $r_2$, $\varepsilon$, $\sigma_1$, $\sigma_2$, $\sigma$, $p$, $N$.

1: Initialization: $i = 0$, $u^0 = f$.
2: **while** $i \leq N$ **do**
3: Calculate the adaptive function $\alpha = \frac{|u_\sigma^i|^p}{|\max(u_\sigma^i)|^p}$.
4: Calculate the reference image $g = \mathcal{D}_{\sigma_1}(u^i)$.
5: Run Algorithm 1 with input $f$, $g$, $\alpha$, $\mu$, $\eta$, $r_1$, $r_2$, and $\varepsilon$. Denote the output by $u^{i+1}$.
6: $i = i + 1$.
7: **end while**
8: Let $u = \mathcal{D}_{\sigma_2}(u^N)$.
9: **return** The restored image $u$.

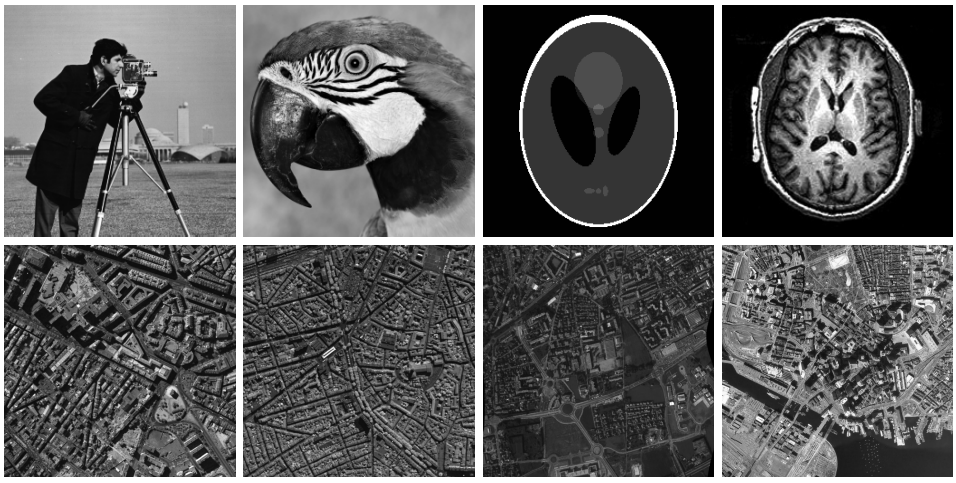

FIGURE 2. Test images. First row: Standard test images Cameraman, Parrot, Phantom, Brain; Second row: Aerial images A1, A2, A3, A4.

4. **Numerical simulation.** In this section, numerical experiments are presented to demonstrate the performance of the proposed Alg. 2 for removing multiplicative noise. We deploy the well-known Gaussian denoiser BM3D [9] for Alg. 2 since it provides state-of-the-art image restoration results with acceptable running time. It is also necessary to consider the recent learning-based algorithm for Alg. 2. We select DnCNN [31]. [1]

A set of 8-bit images with different features shown in Figure 2 are selected for the simulation. We consider the image restoration problem under multiplicative noise with $L = 1, 4, 10$. The larger the parameter $L$, the more heavily contaminated the image. The quality of the restored images is evaluated by both the peak signal-to-noise ratio (PSNR) and the structural similarity index (SSIM) [30]. The codes are running on a desktop equipped with an Intel Core i7 3.20 GHz CPU.

[1] We use the codes provided by the authors. BM3D: https://webpages.tuni.fi/foi/GCF-BM3D/. DnCNN: https://github.com/cszn/DnCNN.

TABLE 1. Parameter setting for Alg. 2.

| $L$ | $\eta$ | $\mu$ | $\sigma_1$ | $\sigma_2$ | $N$ | $r_1$ | $r_2$ | $\varepsilon$ | $\sigma$ | $p$ |
|---|---|---|---|---|---|---|---|---|---|---|
| 1 | 250 | 0.05 | +15 | +5 | 10 | | | | | |
| 4 | 300 | 0.12 | +4 | +0 | 5 | 0.1 | 0.3 | $10^{-5}$ | 1 | 3 |
| 10 | 500 | 0.15 | +3 | +0 | 5 | | | | | |

4.1. **Parameter setting.** Alg. 2 contains a few parameters that need to be adjusted manually. Fortunately, some of them (i.e., $r_1, r_2, \varepsilon, \sigma, p$) are robust to the test image and the noise level. For simplicity of implementation, we set the remaining parameters (i.e., $\eta, \mu, \sigma_1, \sigma_2, N$) as functions of $L$. Table 1 lists the setting of these parameters. In the following, we briefly discuss the guideline for the selection of these parameters.

Let us first consider the model parameter in the energy functional (5). The parameters $\eta$ and $\mu$ leverage the influence of the Gaussian denoiser and the data fidelity term respectively. The stronger the noise, the lower the reliability of $g$ and $f$. Consequently, both $\eta$ and $\mu$ shall increase with the increase of the parameter $L$ (i.e., the decrease of the noise level). The parameters $\sigma$ and $p$ control the adaptive function $\alpha(x)$ in the adaptive TV regularizer. Figure 3 shows the relation between the denoising results (in terms of PSNR) and the four parameters for four test images. In each subplot, we fix all parameters according to Table 1 except the one we are interested in. It is observed that both $\sigma$ and $p$ are not sensitive to the test image. Although the results of parameters $\eta$ and $\mu$ show some differences for different test images, we can still find appropriate values for them according to the subplots in Figure 3.

The utilization of the augmented Lagrangian method introduces two algorithm parameters $r_1$ and $r_2$ that influence the convergence of the algorithm and the computational speed. A small constant $\varepsilon$ is also introduced for the stopping criteria. All of them are fixed throughout this section. The proposed model (5) is convex only if the assumption $\frac{\eta}{\mu} \leq 27 \inf_\Omega |f|^2$ is satisfied. We numerically verify the convergence of Alg. 1 for different $N$ in Figure 4.

Generally, the proposed Alg. 2 does not converge as $N \to \infty$. This is due to the fact that the denoiser $\mathcal{D}$ update the reference image $g$ for each $N$. We also observe from Figure 4 that the object functional (5) has the lowest energy when $N = 1$. The parameter $N$ should be chosen as a decreasing function of $L$.

At last, let us consider the Gaussian denoiser and its parameter. The parameter depends on the standard deviation of the noise and controls the strength of the denoising. It should be a decreasing function of $L$ and also a decreasing function of $N$. Roughly speaking, we are able to estimate the standard deviation of the noise for images corrupted by multiplicative noise and let it be the parameter for the selected Gaussian denoiser. Numerical observations indicate that an appropriate adjustment of it improves the results dramatically. Throughout this paper, we estimate the standard deviation of the noise by [16] and adjust it manually to achieve the best restoration results. The proposed algorithm utilizes the Gaussian denoiser twice. Different parameters should be used.

4.2. **Image restoration results.** Since we utilize BM3D as the Gaussian denoiser for Alg. 2, we evaluate and compare the performance of Alg. 2 with

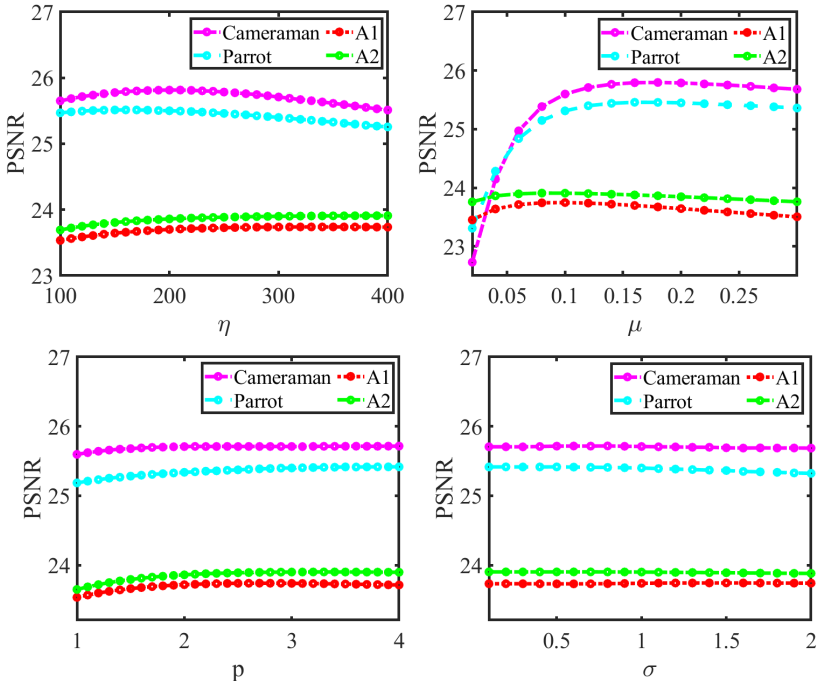


FIGURE 3. The PSNR values of Alg. 2 with the denoiser BM3D for four test images. The noise level $L = 4$.

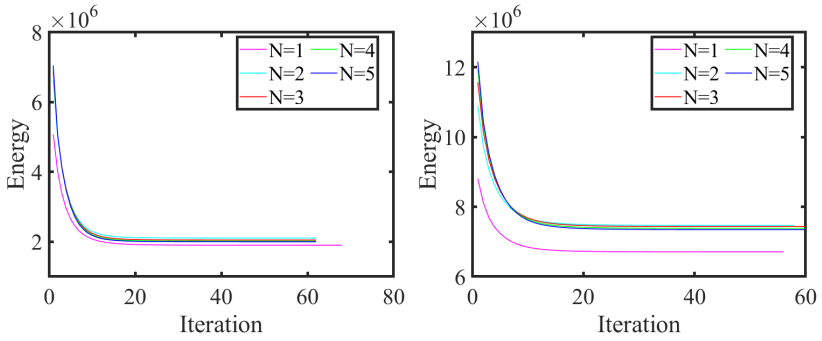


FIGURE 4. The convergence of Alg. 1 with the denoiser BM3D for test images Cameraman (left) and A1 (right) with $L = 4$.

- AA model (1): A classical variational algorithm based on the TV regularization;
- FANS [8]: A fast adaptive nonlocal SAR despeckling algorithm based on BM3D;
- MuLoG [10]: An image despeckling algorithm that utilizes an off-the-shelf Gaussian denoiser. We let BM3D be the denoiser.

The parameter $\eta$ in AA model (1) and the parameter $L$ in FANS are manually tuned to achieve the highest PSNR values. To study the role of the adaptive TV

regularization in our model, we consider RED (i.e., Alg. 2 with $\alpha(x) \equiv 0$) for multiplicative noise removal. More precisely, we update $u^{k+1}$ in Alg. 2 by solving

$$0 = \mu(u - g)) + \eta \frac{f - u}{g^2},$$

where we once again use the reference image $g$ to approximate the denominator of the second term.

4.2.1. *Comparison with other algorithms.* Let us first consider Alg. 2 with BM3D. In Table 2 and Table 3 we list the PSNR and SSIM values of different algorithms for images corrupted by multiplicative noise with $L = 1, 4, 10$. The highest values (excluding DnCNN) are shown in boldface. From the results of AA and Alg. 2 we observe that the new quadratic penalty term improves the image restoration performance dramatically. MuLoG and FANS have similar results for $L = 4, 10$. MuLoG outperforms FANS when $L = 1$. The proposed Alg. 2 obtains the highest PSNR and SSIM values (on average). Although Alg. 2 has lower PSNR values in individual cases, they are very close to the highest values. We notice from the results of RED that the utilization of the adaptive TV regularization for Alg. 2 improves the denoising results by about 0.2 dB.

The restored images shown in Figure 5 clearly illustrate the advantage of Alg. 2, i.e., avoiding the artificial effects caused by RED. Figure 6 indicates that MuLoG, RED, and Alg. 2 achieve better visual quality than AA and FANS for aerial images. The results of MuLoG, RED, and Alg. 2 are close. But we can still see that Alg. 2 tends to suppress bright pixels. Sometimes the bright pixels truly exist in the test image (see the test images A2 and A3), and sometimes the bright pixels are caused by noise (see the test image A1). Noticing that TV regularization also has the effect of suppressing bright pixels (see the results of AA model in Figure 6), this once again verifies that Alg. 2 inherits the characteristics of TV regularization.

Table 4 presents the average running time for five algorithms. The gradient descent scheme is used for AA model. So it is the most time-consuming. MuLoG and RED take about the same amount of running time. Compared to RED, the ADMM algorithm is called 5 to 10 times by Alg. 2 for each experiment. Thus Algorithm 2 consumes more time. It should be noticed that utilizing different algorithm parameters $r_1$ and $r_2$ for different images shall reduce the running time for Alg. 2.

4.2.2. *Comparison of different image denoisers.* After discussing the performance of Alg. 2 with denoiser BM3D, it is straightforward to consider the recent learning-based algorithm DnCNN for Alg. 2.

In Table 2 and Table 3, we also list the PSNR and SSIM values of Alg. 2 with DnCNN (denoted by 'DnCNN'). By observing the results of the four test images A1-A4, we find that in the framework of Alg. 2, DnCNN has an advantage when processing low-noise (i.e., large $L$) images. BM3D, on the other hand, is better at handling high-noise images (i.e., small $L$). Now let us consider the first four test images. We find no pattern in the results of BM3D and DnCNN. Sometimes DnCNN outperforms BM3D (see Phanton with $L = 1$) by a large margin, and sometimes the opposite is true (see Parrot with $L = 4$). We believe the reason for the above phenomenon is that the model-based algorithm BM3D is more robust than the learning-based algorithm DnCNN, especially when the noise does not follow the Gaussian distribution.

TABLE 2. PSNR values of the image restoration results for different algorithms.

| Image | C.man | Parrot | Phantom | Brain | A1 | A2 | A3 | A4 | Avg. |
|---|---|---|---|---|---|---|---|---|---|
| | | | | | $L = 1$ | | | | |
| AA | 20.20 | 18.67 | 19.05 | 17.02 | 18.45 | 18.97 | 22.36 | 16.77 | 18.94 |
| FANS | 22.29 | 20.98 | 22.82 | 19.61 | 20.01 | 19.96 | 22.07 | 18.17 | 20.74 |
| MuLoG | 22.26 | 21.94 | 24.60 | 19.21 | 20.78 | 20.56 | 23.87 | 18.25 | 21.43 |
| RED | 22.12 | 22.01 | **24.91** | 20.53 | 20.85 | 20.62 | 23.82 | 18.34 | 21.65 |
| Alg. 2 | **22.32** | **22.16** | 24.67 | **20.54** | **20.92** | **20.74** | **23.88** | **18.45** | **21.71** |
| DnCNN | 22.74 | 22.18 | 25.56 | 20.69 | 20.75 | 20.51 | 23.43 | 18.34 | 21.78 |
| | | | | | $L = 4$ | | | | |
| AA | 23.71 | 21.94 | 22.59 | 18.80 | 21.67 | 21.71 | 24.76 | 19.50 | 21.83 |
| FANS | 25.18 | 24.45 | 27.39 | 22.86 | 23.11 | 23.08 | 26.04 | 20.64 | 24.09 |
| MuLoG | **25.77** | 24.58 | 26.95 | 22.33 | 23.62 | 23.70 | 26.69 | 20.57 | 24.28 |
| RED | 25.68 | 25.06 | 27.45 | 23.49 | 23.55 | 23.84 | 26.65 | 20.71 | 24.55 |
| Alg. 2 | 25.71 | **25.40** | **27.66** | **23.60** | **23.74** | **23.90** | **26.81** | **20.77** | **24.70** |
| DnCNN | 25.32 | 24.44 | 27.32 | 22.99 | 23.83 | 23.94 | 27.12 | 20.77 | 24.47 |
| | | | | | $L = 10$ | | | | |
| AA | 25.84 | 22.49 | 24.59 | 19.08 | 24.13 | 24.26 | 27.01 | 21.63 | 23.63 |
| FANS | 27.33 | 26.65 | 30.15 | 25.35 | 25.53 | 25.58 | 28.72 | **22.49** | 26.48 |
| MuLoG | 27.79 | 26.37 | 29.55 | 24.58 | **25.86** | 26.03 | 28.98 | 22.45 | 26.45 |
| RED | 27.89 | 26.57 | 30.23 | 25.60 | 25.46 | 26.00 | 28.84 | 22.35 | 26.62 |
| Alg. 2 | **27.95** | **27.39** | **30.51** | **25.77** | 25.81 | **26.11** | **29.02** | 22.47 | **26.88** |
| DnCNN | 27.92 | 27.23 | 29.45 | 25.51 | 26.22 | 26.34 | 29.36 | 22.76 | 26.85 |

TABLE 3. SSIM values of the image restoration results for different algorithms.

| Image | C.man | Parrot | Phantom | Brain | A1 | A2 | A3 | A4 | Avg. |
|---|---|---|---|---|---|---|---|---|---|
| | | | | | $L = 1$ | | | | |
| AA | 0.632 | 0.597 | 0.701 | 0.697 | 0.647 | 0.601 | 0.598 | 0.514 | 0.623 |
| FANS | 0.692 | 0.655 | 0.764 | 0.673 | 0.760 | **0.747** | **0.678** | 0.613 | 0.698 |
| MuLoG | 0.681 | 0.702 | **0.951** | 0.770 | 0.745 | 0.699 | 0.652 | 0.623 | 0.728 |
| RED | 0.690 | **0.708** | 0.926 | 0.781 | 0.756 | 0.711 | 0.658 | 0.643 | 0.734 |
| Alg. 2 | **0.698** | **0.708** | 0.923 | **0.788** | **0.765** | 0.727 | 0.665 | **0.661** | **0.742** |
| DnCNN | 0.733 | 0.712 | 0.893 | 0.775 | 0.761 | 0.708 | 0.656 | 0.631 | 0.734 |
| | | | | | $L = 4$ | | | | |
| AA | 0.736 | 0.736 | 0.802 | 0.728 | 0.857 | 0.857 | 0.793 | 0.761 | 0.784 |
| FANS | **0.787** | 0.786 | 0.967 | 0.824 | 0.891 | 0.893 | **0.862** | 0.814 | 0.853 |
| MuLoG | 0.782 | 0.789 | 0.973 | 0.866 | 0.883 | 0.883 | 0.843 | 0.804 | 0.853 |
| RED | 0.775 | 0.791 | 0.973 | 0.868 | 0.892 | 0.894 | 0.852 | **0.817** | 0.858 |
| Alg. 2 | 0.785 | **0.793** | **0.974** | **0.872** | **0.895** | **0.895** | 0.854 | 0.814 | **0.860** |
| DnCNN | 0.771 | 0.774 | 0.967 | 0.858 | 0.898 | 0.897 | 0.866 | 0.822 | 0.857 |
| | | | | | $L = 10$ | | | | |
| AA | 0.786 | 0.775 | 0.946 | 0.738 | 0.927 | 0.929 | 0.884 | 0.868 | 0.856 |
| FANS | **0.836** | 0.840 | 0.983 | 0.895 | 0.940 | 0.942 | **0.924** | **0.895** | **0.907** |
| MuLoG | 0.825 | 0.835 | 0.983 | **0.908** | 0.939 | 0.943 | 0.917 | 0.888 | 0.905 |
| RED | 0.827 | 0.823 | 0.983 | 0.904 | 0.939 | 0.944 | 0.918 | 0.885 | 0.903 |
| Alg. 2 | 0.833 | **0.847** | **0.984** | 0.906 | **0.941** | **0.945** | 0.919 | 0.885 | **0.907** |
| DnCNN | 0.826 | 0.843 | 0.970 | 0.894 | 0.945 | 0.946 | 0.926 | 0.900 | 0.906 |

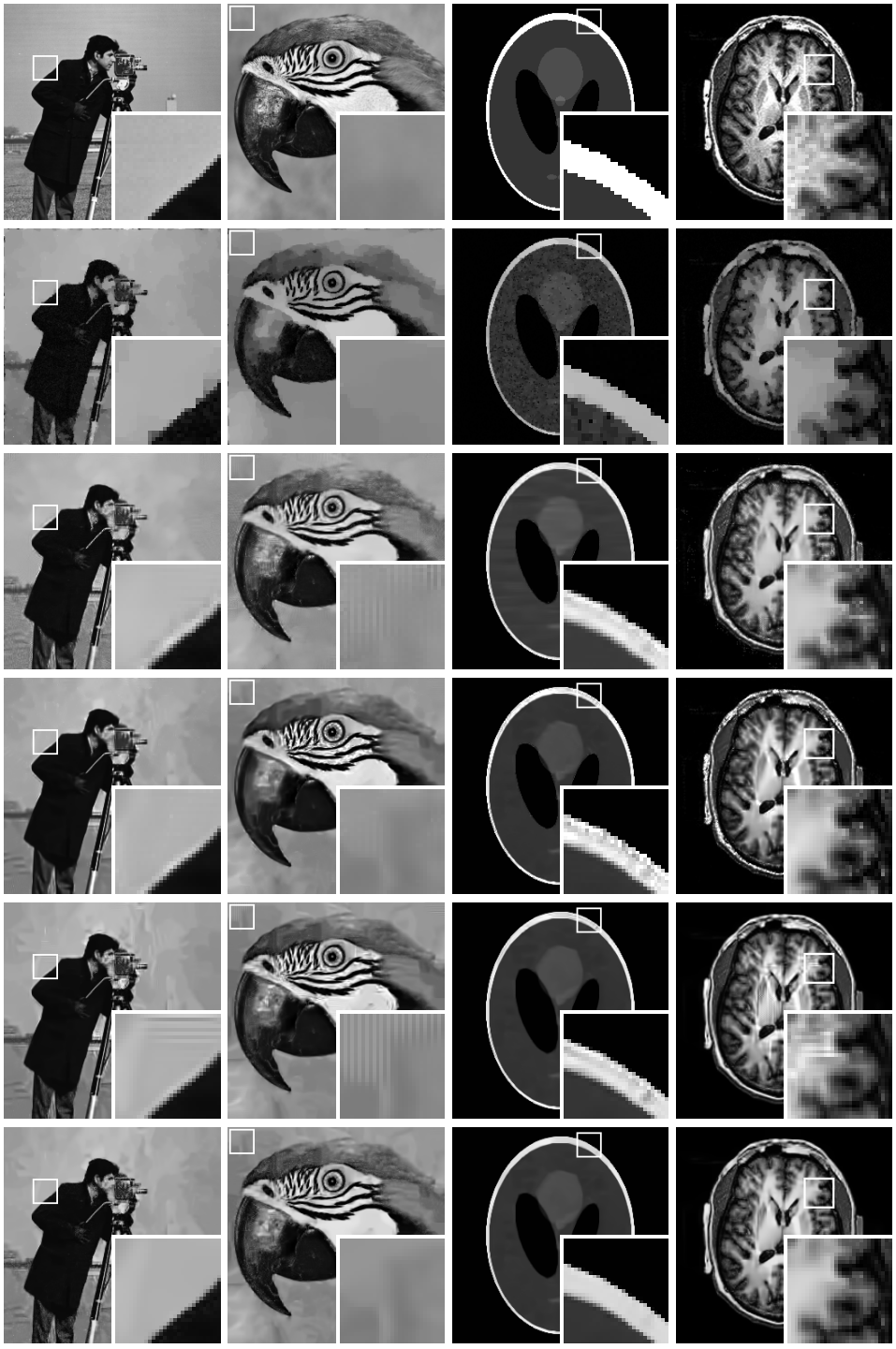

FIGURE 5. The restored results of different algorithms for four test images with $L = 4$. From top to bottom: Original image, AA, FANS, MuLoG, RED, Alg. 2.

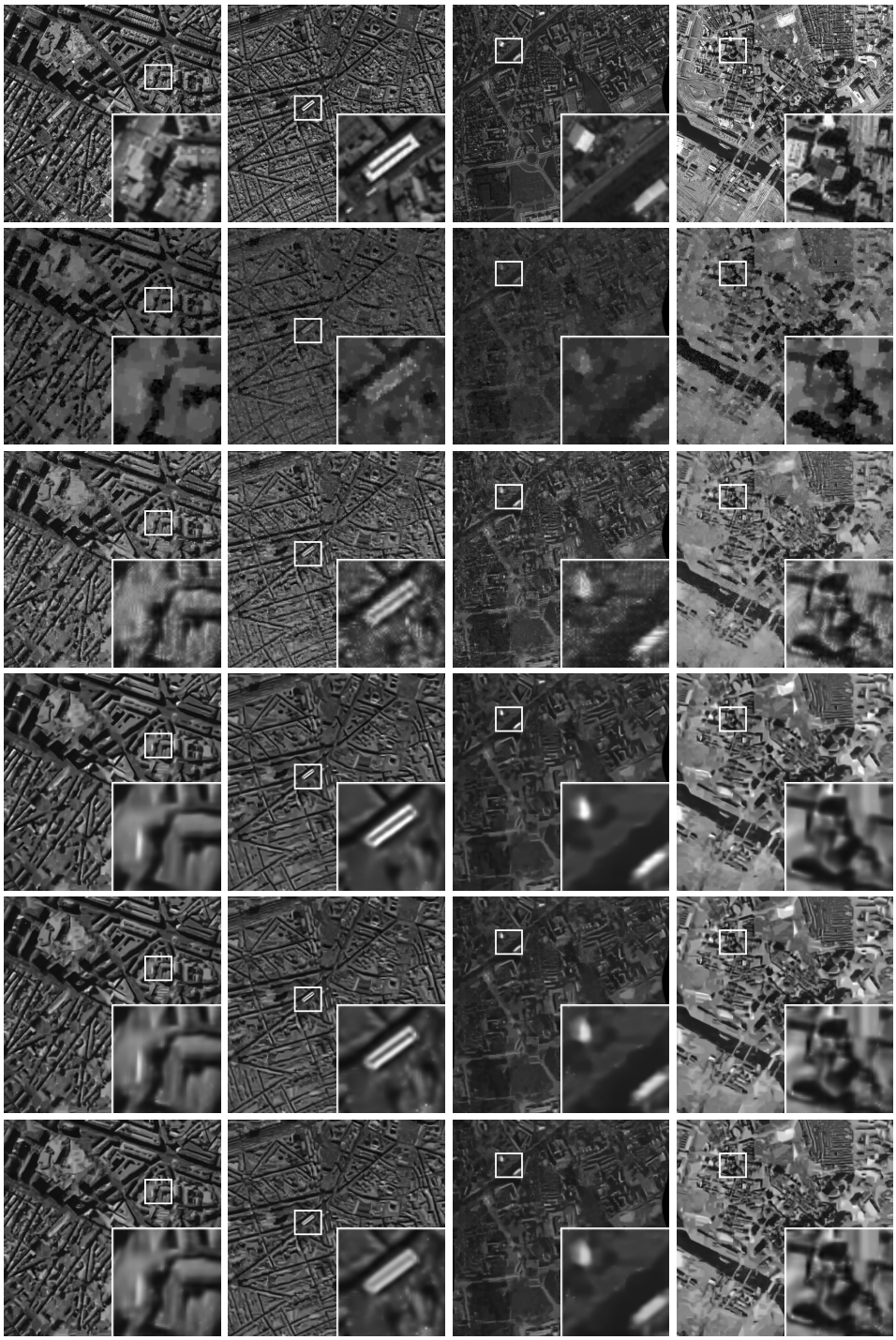

FIGURE 6. The restored results of different algorithms for four test images with $L = 1$. From top to bottom: Original image, AA, FANS, MuLoG, RED, Alg. 2.

TABLE 4. The average running time in seconds for all test images and noise levels.

| Algorithm | AA | FANS | MuLoG | RED | Alg. 2 |
|---|---|---|---|---|---|
| Time | 30.0 | 5.0 | 11.5 | 11.4 | 17.1 |

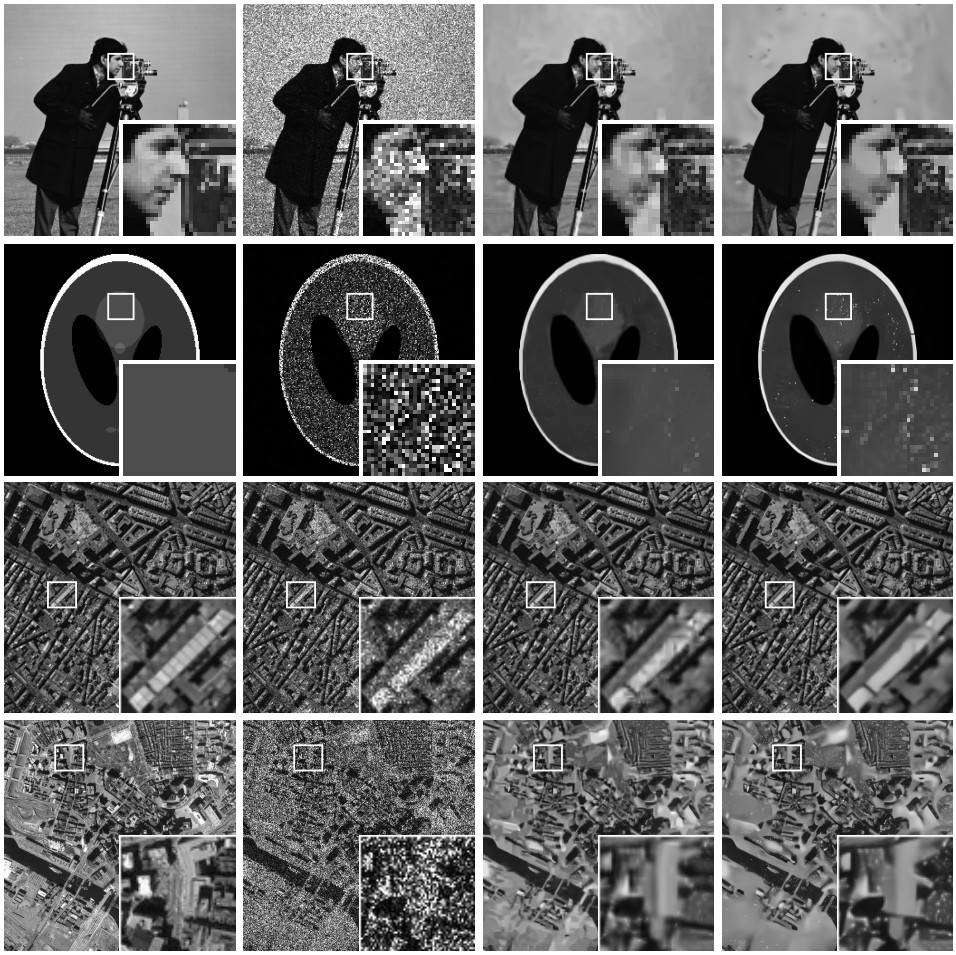

FIGURE 7. Restoration results of Alg. 2 with denoisers BM3D and DnCNN. From left to right: Original image, noisy image, BM3D, DnCNN. From top to bottom: Camerman with $L = 10$, Phantom with $L = 1$, A1 with $L = 10$, A4 with $L = 1$.

Figure 7 shows us the difference between BM3D and DnCNN for Alg. 2. As we can see from the results of the test images Cameraman and A1 ($L = 10$), DnCNN creates better visual quality than BM3D in restoring details. The results of the test images Phantom and A4 ($L = 1$) demonstrate the disadvantage of DnCNN. It can not suppress white speckles in the images. In summary, we suggest the state-of-the-art model-based Gaussian denoiser for Alg. 2. More advanced learning-based

Gaussian denoisers can also be considered for Alg. 2 if the noise is not strong and the original image does not contain many bright pixels.

5. **Conclusion.** In this paper, we proposed a convex variational model that combines the adaptive TV regularization and the Regularization by Denoising (RED) for the removal of multiplicative noise. The existence and uniqueness of solutions for the proposed model were proved. The alternating direction method of multiplier (ADMM) was carried out for solving the model. The effectiveness of the proposed method was verified through numerical experiments.

**Acknowledgments.** This work was funded by National Natural Science Foundation of China (12001509) and China Scholarship Council.

## REFERENCES

[1] G. Aubert and J.-F. Aujol, A variational approach to removing multiplicative noise, *SIAM journal on applied mathematics*, **68** (2008), 925–946.
[2] G. Aubert, P. Kornprobst and G. Aubert, *Mathematical problems in image processing: partial differential equations and the calculus of variations*, vol. 147, Springer, 2006.
[3] S. Boyd, N. Parikh, E. Chu, B. Peleato, J. Eckstein et al., Distributed optimization and statistical learning via the alternating direction method of multipliers, *Foundations and Trends® in Machine learning*, **3** (2011), 1–122.
[4] G. Carlier and M. Comte, On a weighted total variation minimization problem, *Journal of Functional Analysis*, **250** (2007), 214–226.
[5] A. Chambolle and T. Pock, A first-order primal-dual algorithm for convex problems with applications to imaging, *Journal of mathematical imaging and vision*, **40** (2011), 120–145.
[6] T. F. Chan and J. Shen, Variational image inpainting, *Communications on Pure and Applied Mathematics: A Journal Issued by the Courant Institute of Mathematical Sciences*, **58** (2005), 579–619.
[7] Y. Chen and T. Wunderli, Adaptive total variation for image restoration in bv space, *Journal of Mathematical Analysis and Applications*, **272** (2002), 117–137.
[8] D. Cozzolino, S. Parrilli, G. Scarpa, G. Poggi and L. Verdoliva, Fast adaptive nonlocal sar despeckling, *IEEE Geoscience and Remote Sensing Letters*, **11** (2013), 524–528.
[9] K. Dabov, A. Foi, V. Katkovnik and K. Egiazarian, Image denoising by sparse 3-d transform-domain collaborative filtering, *IEEE Transactions on image processing*, **16** (2007), 2080–2095.
[10] C.-A. Deledalle, L. Denis, S. Tabti and F. Tupin, Mulog, or how to apply gaussian denoisers to multi-channel sar speckle reduction?, *IEEE Transactions on Image Processing*, **26** (2017), 4389–4403.
[11] G. Dong, Z. Guo and B. Wu, A convex adaptive total variation model based on the gray level indicator for multiplicative noise removal, in *Abstract and Applied Analysis*, vol. 2013, Hindawi, 2013.
[12] Y. Dong and T. Zeng, A convex variational model for restoring blurred images with multiplicative noise, *SIAM Journal on Imaging Sciences*, **6** (2013), 1598–1625.
[13] X. Feng and X. Zhu, Models for multiplicative noise removal, *Handbook of Mathematical Models and Algorithms in Computer Vision and Imaging: Mathematical Imaging and Vision*, 1–34.
[14] M. Gao, B. Kang, X. Feng, W. Zhang and W. Zhang, Anisotropic diffusion based multiplicative speckle noise removal, *Sensors*, **19** (2019), 3164.
[15] T. Goldstein and S. Osher, The split bregman method for l1-regularized problems, *SIAM journal on imaging sciences*, **2** (2009), 323–343.
[16] J. Immerkaer, Fast noise variance estimation, *Computer vision and image understanding*, **64** (1996), 300–302.
[17] S. Majee, R. K. Ray and A. K. Majee, A gray level indicator-based regularized telegraph diffusion model: application to image despeckling, *SIAM Journal on Imaging Sciences*, **13** (2020), 844–870.
[18] C. Oliver and S. Quegan, *Understanding synthetic aperture radar images*, SciTech Publishing, 2004.

[19] Y. Romano, M. Elad and P. Milanfar, The little engine that could: Regularization by denoising (red), *SIAM Journal on Imaging Sciences*, **10** (2017), 1804–1844.
[20] L. I. Rudin, S. Osher and E. Fatemi, Nonlinear total variation based noise removal algorithms, *Physica D: nonlinear phenomena*, **60** (1992), 259–268.
[21] J. M. Schmitt, S. Xiang and K. M. Yung, Speckle in optical coherence tomography, *Journal of biomedical optics*, **4** (1999), 95–105.
[22] F. Sciacchitano, Y. Dong and T. Zeng, Variational approach for restoring blurred images with cauchy noise, *SIAM Journal on Imaging Sciences*, **8** (2015), 1894–1922.
[23] X. Shan, J. Sun and Z. Guo, Multiplicative noise removal based on the smooth diffusion equation, *Journal of Mathematical Imaging and Vision*, **61** (2019), 763–779.
[24] J. Shen, S. H. Kang and T. F. Chan, Euler's elastica and curvature-based inpainting, *SIAM journal on Applied Mathematics*, **63** (2003), 564–592.
[25] G. Steidl and T. Teuber, Removing multiplicative noise by douglas-rachford splitting methods, *Journal of Mathematical Imaging and Vision*, **36** (2010), 168–184.
[26] D. M. Strong and T. F. Chan, Spatially and scale adaptive total variation based regularization and anisotropic diffusion in image processing, in *Diusion in Image Processing, UCLA Math Department CAM Report*, Citeseer, 1996.
[27] X.-C. Tai, J. Hahn and G. J. Chung, A fast algorithm for euler's elastica model using augmented lagrangian method, *SIAM Journal on Imaging Sciences*, **4** (2011), 313–344.
[28] S. V. Venkatakrishnan, C. A. Bouman and B. Wohlberg, Plug-and-play priors for model based reconstruction, in *2013 IEEE Global Conference on Signal and Information Processing*, IEEE, 2013, 945–948.
[29] R. F. Wagner, Statistics of speckle in ultrasound b-scans, *IEEE Trans. Sonics & Ultrason.*, **30** (1983), 156–163.
[30] Z. Wang, A. C. Bovik, H. R. Sheikh and E. P. Simoncelli, Image quality assessment: from error visibility to structural similarity, *IEEE transactions on image processing*, **13** (2004), 600–612.
[31] K. Zhang, W. Zuo, Y. Chen, D. Meng and L. Zhang, Beyond a gaussian denoiser: Residual learning of deep cnn for image denoising, *IEEE transactions on image processing*, **26** (2017), 3142–3155.
[32] T. Zhang, J. Chen, C. Wu, Z. He, T. Zeng and Q. Jin, Edge adaptive hybrid regularization model for image deblurring, *Inverse Problems*, **38** (2022), 065010.
[33] Y. Zhang, S. Li, Z. Guo, B. Wu and S. Du, Image multiplicative denoising using adaptive euler's elastica as the regularization, *Journal of Scientific Computing*, **90** (2022), 1–34.